



Localize surface plasmon resonance of silver nanoparticles using Mie theory

F. Y. Alzoubi¹, Ahmad A. Ahmad¹, Ihsan A. Aljarrah¹, A. B. Migdadi¹, and Qais M. Al-Bataineh^{2,3,*} 

¹ Department of Physical Sciences, Jordan University of Science & Technology, P.O. Box 3030, Irbid 22110, Jordan

² Leibniz Institut für Analytische Wissenschaften-ISA-e.V, Bunsen-Kirchhoff-Straße 11, 44139 Dortmund, Germany

³ Experimental Physics, TU Dortmund University, 44227 Dortmund, Germany

Received: 28 May 2023

Accepted: 11 September 2023

Published online:
9 November 2023

© The Author(s), 2023

ABSTRACT

In this work, the optical properties of silver nanoparticles (AgNPs) were explored using Mie theory compared with the experimental AgNPs using the chemical reduction method. Mie's theory is suited for accurately evaluating the scattering, absorption, and extinction cross-sections of spherical AgNPs. Therefore, the wavelength of localized surface plasmon resonance (LSPR) in the optical spectra of the spherical AgNPs was calculated. The experimental AgNPs have a spherical shape with an average particle size of 30 nm. In addition, the crystalline structure of AgNPs was found to be cubic with *fcc* structure with lattice constant $a = 4.155$ Å. Moreover, the excitation of the LSPR of the AgNPs was simulated using the finite-difference time-domain (FDTD) method at different wavelengths to explore the LSPR phenomena. The results show that spherical AgNPs are the most widely used materials in biosensors, biomedicine, optoelectronic devices, and solar cells due to their surface plasmon resonances in the visible spectrum region.

1 Introduction

Metallic nanostructures have lately attracted attention due to their large surface area to volume ratio and the quantum confinement effects, which affect the physical and chemical properties, such as the optical, electrical, and catalytic properties, and increase their ability to interact with their surroundings [1]. Also, due to the large surface area and the quantum effects, there is a variation in the properties of the nanoparticles compared to the bulk material giving them unique characteristics compared to the conventional particles [2, 3]. In general, the properties of metallic nanoparticles depend on their size, shape, and crystal structure [4]. Among these metallic nanostructures,

silver nanoparticles (AgNPs) have unique physical and chemical properties compared to others, including optical, excellent thermal stability, high electrical conductivity, and antimicrobial [5, 6]. These properties made them useful in various daily activities, including medical, therapeutic, health care, food, and industrial applications [5]. Silver nanoparticles efficiently absorb, and scatter light, and the color of colloidal AgNPs depends on their size and shape [7].

Moreover, the localized surface plasmon resonance (LSPR) band characterizes the optical spectra of the metal nanoparticles (MNPs) [8]. LSPR is a collective oscillation of the electron density at the metal/medium interface revealed from the incident photons—MNP interactions which induce an electric field at the

Address correspondence to E-mail: qais.al-bataineh@isas.de

interface [9, 10]. The LSPR peak of light occurs when the incident photons' frequency matches the surface plasmons' natural frequency, and the result appears as an absorption peak in the absorption spectrum [11, 12]. This phenomenon is helpful in various applications, such as biosensors, biomedicine, optoelectronic devices, and solar cells [13, 14]. The outcomes of the phenomenon release surface radiation through Mie scattering or may even converge to thermal energy [15]. The MNPs characteristics, including structure dimensions, metallic nan composition, and the surface ambient, designated the nature of the LSPR [16]. Also, the LSPR of MNPs is characterized by the absorption and scattering of incident light at specific wavelengths depending on different parameters such as the nanoparticles' size, shape, and dielectric environment [17]. For example, the resonant frequency will change because any alteration to the metal particle's shape or size will modify how free electrons oscillate [18].

Theoretical and experimental investigations of the optical properties of the MNPs are of the essential need for investigating the dynamical phenomenology of scattering and absorbing light [19]. Mie's theory has been used to explore the light scattering and absorption caused by spherical nanoparticles by solving Maxwell's equations [15]. Mie's theory characterizes the interactions of the electromagnetic waves with the MNPs at the boundaries of the surfaces. The complex permittivity of the MNPs evaluated by Drude's theory is also an essential parametric function for calculating the light scattering and absorption caused by the spherical nanoparticle [20].

Silver nanoparticles (AgNPs) received a great deal of interest due to their exceptionally significant absorption coefficient and extinction coefficient, which reveal biosensing platforms in the visible spectrum range [21]. The spherical AgNPs acquire distinct LSPR bands in the visible region (blue light, in particular) [22], which can be adjusted by modifying their nano size and non-structural shapes [23]. One typical example is that spherical AgNPs only exhibit one surface SPR band, but triangular AgNPs show three SPR bands corresponding to dipole and quadrupole plasmon resonance [24]. Further, some previous studies revealed that the position of the LSPR peak exhibited a red shifting from 390 to 460 nm as a result of an increase in AgNPs size [25]. According to the literature, colloidal AgNPs in deionized water exhibit LSPR peaks ranging from 380 to 460 nm, typical of monodispersed silver nanoparticles

with an average diameter of less than 100 nm [26]. Spherical AgNPs with about 30–40 nm diameter have the LSPR peak at ~ 400 nm, giving the colloidal a distinctive yellow color. AgNPs are particularly desirable for surface plasmon applications due to their considerable enhancement of near fields compared to gold nanoparticles, where the signal improvement obtained from silver nanoparticles is most noticeable when the LSPR is activated by the incident light under a resonant situation [27, 28]. Additionally, compared to other metal films, silver nanofilms are more responsive to changes in the medium around them [29]. As reported, the LSPR of AgNPs has a significant role in several applications, including nanophotonic devices, surface-enhanced fluorescence (SEF), and surface-enhanced Raman scattering (SERS) [30]. Furthermore, SPR peak positions can be used as detectors for low quantities of interesting biological compounds because of their sensitivity to slight changes in the dielectric environment [31]. In this work, LSPR parameters, particularly the light scattering, and absorption that occurred due to the AgNPs, were investigated and explored using the Mie theory and the modified Drude theory compared to the experimentally measured outcomes.

2 Theoretical backgrounds

2.1 Localized surface plasmon resonance

The resonance absorption and scattering bands of the MNPs in the visible region are related to the collective oscillation of the electron density at the metal/medium interface, resulting from the light wave's interaction with the MNPs. Plasma frequency ($\omega_p = \sqrt{4\pi ne^2/m}$) is a crucial property of MNPs. The incident electric field (E) of the electromagnetic light wave interrupts the cloud of the freely distributed electrons revealing an ambient around the MNPs of uncompensated charges, as seen in Fig. 1. As a result of the light-MNPs interaction, a coherent vibrational oscillation occurred to the electron cloud around the MNPs' surface caused by the reflected forces from the uncompensated charges [8]. Figure 1 shows the block diagram of the unperturbed electron cloud, which has been disturbed by the incident electric field of the light wave causing coherent localized surface plasmon oscillations in the MNPs.

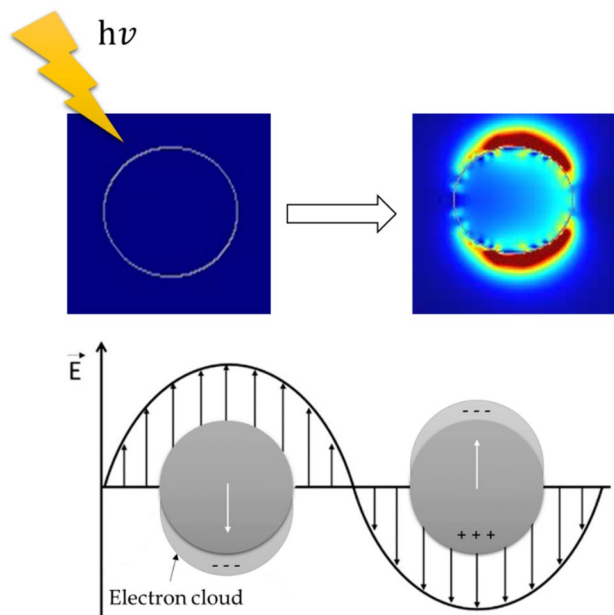


Fig. 1 Schematic diagram of localized plasmon oscillations in MNPs under irradiation of light waves

2.2 Modified drude model

The permittivity of a bulk metal system, which includes the atom’s inner electrons and a monochromatic electric field oscillating with frequency ω , i.e., $E_0 \sim e^{-i\omega t}$ is given by the following equation [19]:

$$\epsilon_{\text{bulk}} = \epsilon_{\infty} - \frac{\omega_p^2}{[\omega^2 + i\Gamma_{\text{bulk}}\omega]}, \tag{1}$$

where: ω_p is the plasma frequency, Γ_{bulk} is the damping factor for bulk metal, and ϵ_{∞} represents the interaction of inner electrons with light,

$$\epsilon_{\infty} = 1 + \sum_{j=1}^{N_0} \frac{\omega_{pj}^2}{(\omega_j^2 - \omega^2) - i\Gamma_j\omega}, \tag{2}$$

where: N_0 is the number of Lorentz oscillators, j presents the special kinds of electrons located at inner levels. In addition, the permittivity of the individual nanoparticle is given by the following equation [19]:

$$\epsilon_{\text{NP}} = \epsilon_{\text{bulk}} + \frac{\omega_p^2}{[\omega^2 + i\Gamma_{\text{bulk}}\omega]} - \frac{\omega_p^2}{[\omega^2 - \alpha\omega_p^2 + i\Gamma_{\text{NP}}\omega]}, \tag{3}$$

where the sum of the first two terms is ϵ_{∞} for the bulk metal, and Γ_{NP} is the damping factor for the nanoparticle.

2.3 Mie theory

Mie’s theory facilitates the investigation of the light wave scattering and absorbing by a spherical MNPs surrounded by a homogeneous medium [32] via solving Maxwell’s equations outside and inside the sphere. Mie’s theory evaluates the absorption and scattering cross-sections of the MNPs and consequently simulates the optical properties of the spherical MNPs [33]. In quasi-static approximation, the scalar potential ($\Delta\Phi = 0$) in the Laplace formula is employed to govern the isotropic polarizability (α) of a spherical NP with specific permittivity (ϵ_1) and radius (a) bounded by a medium with specific permittivity (ϵ_2), as given by [34]:

$$\alpha = 4\pi a^3 \frac{\epsilon_1 - \epsilon_2}{\epsilon_1 + 2\epsilon_2}. \tag{4}$$

The scattering ($C_{\text{sca}}(\omega)$) and absorbing cross sections ($C_{\text{abs}}(\omega)$) are evaluated by knowing the entire dipole radiation and absorption power, according to the following equations [34]:

$$C_{\text{sca}}(\omega) = \frac{k^4}{6\pi} |\alpha(\omega)|, \tag{5}$$

$$C_{\text{abs}}(\omega) = k \text{Im}[\alpha(\omega)], \tag{6}$$

where: k is the incoming wave-vector. Knowing the extinction cross section ($C_{\text{ext}}(\omega)$) as given by: $C_{\text{ext}}(\omega) = C_{\text{sca}}(\omega) + C_{\text{abs}}(\omega)$, Mie theory approximates the polarizability of a sphere with volume (V) as [35, 36]:

$$\alpha = \frac{[1 - 0.1(\epsilon_1 + \epsilon_2)q^2]V_{\text{AuNPs}}}{\left(\frac{\epsilon_2}{\epsilon_1 - \epsilon_2} + \frac{1}{3}\right) - \left[(\epsilon_1 + 10\epsilon_2)\frac{q^2}{30}\right] - 4i\pi^2(\epsilon_2)^{\frac{3}{2}}\frac{V_{\text{AuNPs}}}{3\lambda^3}}, \tag{7}$$

where: q is a dimensionless variable given by:

$$q = \pi \frac{d_{\text{AuNPs}}}{2\lambda}. \tag{8}$$

3 Experimental procedures

Silver nitrate (AgNO_3 , 169.87 g/mol), trisodium citrate ($\text{Na}_3\text{C}_6\text{H}_5\text{O}_7$, 258.06 g/mol), and ascorbic acid ($\text{C}_6\text{H}_8\text{O}_6$, 176.12 g/mol) were all purchased from Sigma-Aldrich. The stock solution was prepared by dissolving 0.01 g of ascorbic acid as a stabilizing agent and 0.88 g of trisodium citrate as a reducing agent in 100 ml of deionized water. Silver nitrate solution was prepared by dissolving 16.987 g of AgNO_3 in 1 ml of deionized water. The stock solution was then placed in a condensation system with continuous stirring at 96 °C. After boiling the solution, 1.0 ml of AgNO_3 solution was added in drop by drop addition until the solution became yellow. The solution was well-maintained, continuously boiling on a stirrer for one hour before cooling down to room temperature [37]. Scanning electron microscopy (Quanta FEG 450, SEM), X-Ray diffraction (Rigaku Ultima IV, XRD), and UV-Vis spectrophotometer (Shimadzu U-3900 H) were used to characterize the resultant silver nanoparticles (AgNPs).

The simulation and theoretical calculations were performed using the finite-difference time-domain (FDTD) method by Lumerical software. First, we design a water medium with a single AgNP in a 2D model. A default design parameter includes incident angle ($\theta = 90^\circ$) and AgNP diameter (range from 30 to 70 nm). The full-field electromagnetic simulations were performed to investigate the local electric field enhancement as well as scattering, absorption, and cross-sectional extinction spectra based on Mie's theory. The base solver directly solves Maxwell's equations in time and space on a spatial grid without simplifying approximations, making the analysis far more

accurate. The vector \mathbf{K} was defined to propagate in the y direction with a polarization mode either in the x - or z -directions (p- and s- polarization, respectively).

4 Results and discussion

According to the SEM image and the size distribution analysis, The AgNPs were spherical within 30 nm nano-size, as seen in the morphological and size distribution analysis in Fig. 2a and b. The powder XRD patterns of the AgNPs exhibit several peaks at 37.5°, 43.6°, and 63.8°, corresponding to the diffraction planes (111), (200), and (220), respectively (Fig. 2c) [37]. These diffraction patterns matched with the silver's face-centered cubic (fcc) structure (JCPDS file No. 04-0783), which indicates mainly an fcc cubic polycrystalline microstructure with preferred (111) orientation. The lattice constant (a) is determined using the equation: $a = \sqrt{3}d_{(111)}$ is 4.155 Å. The UV-Vis absorbance spectrum of AgNPs exhibits a fingerprint peak at 414 nm, corresponding to the surface plasmon resonance of AgNPs (Fig. 2d).

The real and imaginary parts of dielectric permittivity for AgNPs were calculated using modified Drude theory by Maple software. Figure 3 shows the real and imaginary parts of dielectric permittivity for AgNPs dedicated obtained from modified Drude theory by considering only the interband contribution of bound electrons. The interband contribution of bound electrons defers between the real and imaginary part of dielectric permittivity for AgNPs since the real part reflects the dispersion behavior of the material, while the imaginary part refers to the resonance behavior. The vertical dotted line represents the resonant

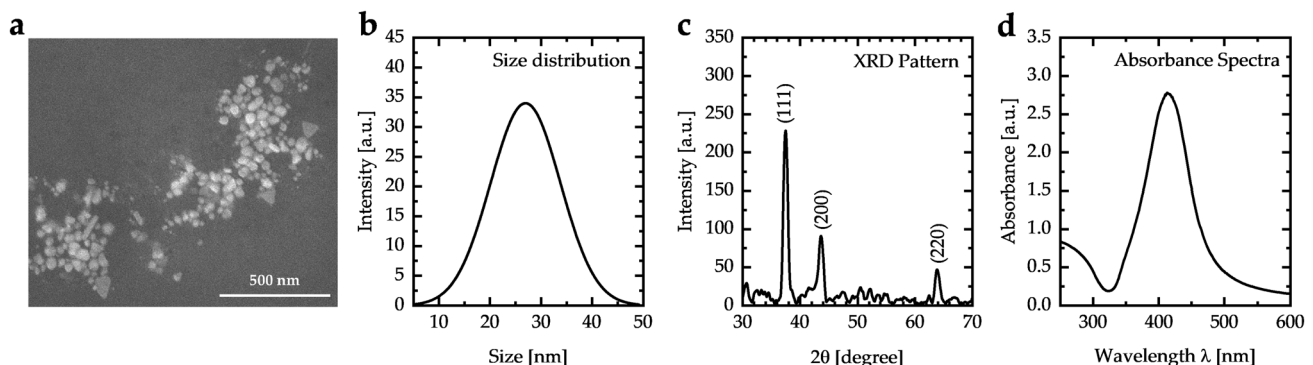


Fig. 2 a SEM micrograph, b size distribution, c XRD patterns, d absorbance spectra of silver nanoparticles (AgNPs)

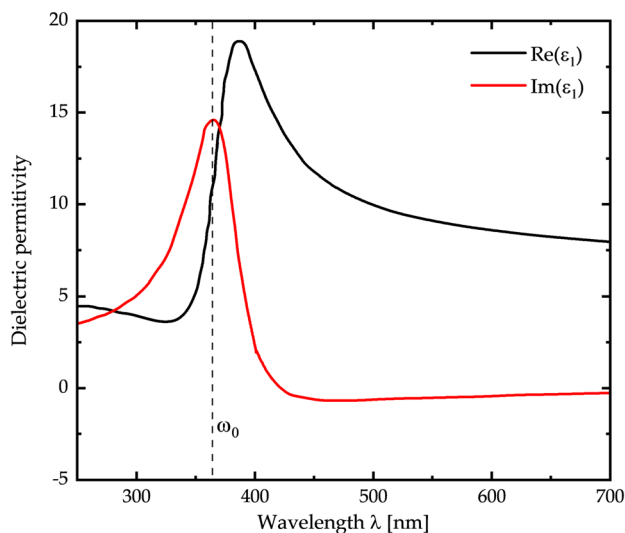


Fig. 3 Contribution of the bound electrons in metal silver to the permittivity

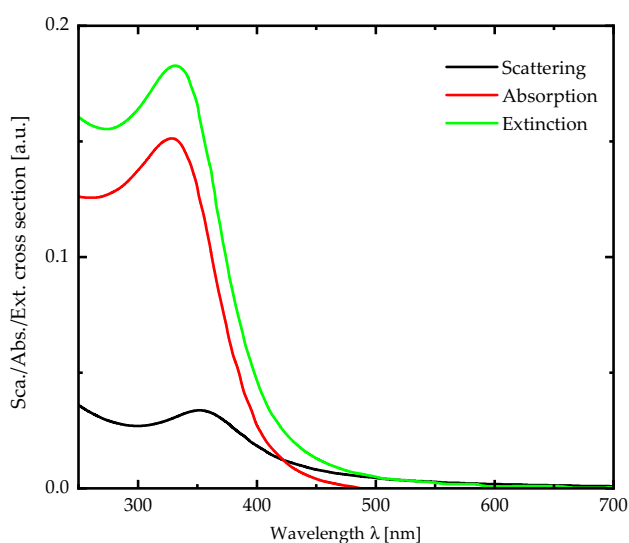


Fig. 4 Analytical optical scattering, absorption, and extinction spectra of 50 nm diameter AgNPs

frequency (ω_0), which is found to be $5.18 \times 10^{15} \text{ s}^{-1}$. The real part of the dielectric permittivity has a single peak at 386 nm, which is a higher wavelength than the main peak in the imaginary part. For a Lorentz oscillator, the real part of permittivity has positive values, while the imaginary part has negative values, a slightly higher wavelength than the resonance wavelength [38].

Figure 4 shows the scattering, absorption, and cross-sectional extinction spectra by 50 nm diameter AgNPs, as calculated using Mie's theory. The scattering and

absorption spectra show resonance interactions at 353 nm and 328 nm, respectively. The extinction cross-section is the sum of scattering and absorption cross-sections. The resonance of the extinction cross-section occurs at 330 nm. In addition, increasing the particle size reveals a shift in the localized surface plasmon resonance wavelength towards the red region. Figure 5 shows the effect of the AgNP size (30, 40, 50, 60, and 70 nm) for different variations in the spectrum. The absorption parameter is generally more robust, broader, and highly redshifted as the sphere diameter is increased, and the least is shown when the 30 diameter spheres are considered. The same behavior was found in a previous study that reported that increasing particle size improved absorption efficiency [39].

The experimental and analytical optical absorbance spectra of the AgNPs with an average size of about 30 nm in a water medium at the same particle size are shown in Fig. 6. The experimental and analytical optical absorbance spectra have different resonance wavelengths attributed to the impurities in a water solution resulting from the preparation process. The theoretical spectrum is concerned with only one Ag nanoparticle [25]. In contrast, the experimental spectrum represents many AgNPs colliding in water and the different distributions of the AgNP sizes compared with the fixed size of one AgNP in the analytical approach [40]. As previously mentioned, the LSPR peak depends on the nanoparticle's size, shape, and surrounding environment, which changes how free electrons oscillate [17, 18]. Additionally, the experimental absorbance spectra show a drop in absorption after the plasmon frequency compared to the simulated data due to low concentrations of AgNPs in the solvent, which means that the solvent absorbance significantly affects the total absorbance spectra [37]. As reported, the dielectric environment affects the LSPR peak and the absorbance spectra of MNPs [17]. T. Gong et al. [41] found and reported the exact behavior of experimental absorbance spectra of silver nanoparticles at 419 nm with an average size of 30 nm and reported the discrepancy of experimental and theoretical spectra is attributed to the ideal conditions that were assumed, such as the AgNPs' uniform diameter and the dipole approximation.

Figure 7 shows the excitation of LSPR of the AgNPs at different times using the finite-difference time-domain (FDTD) method, creating strong electric fields and propagating waves that contribute to light absorption and scattering. Figure 7a and b represent

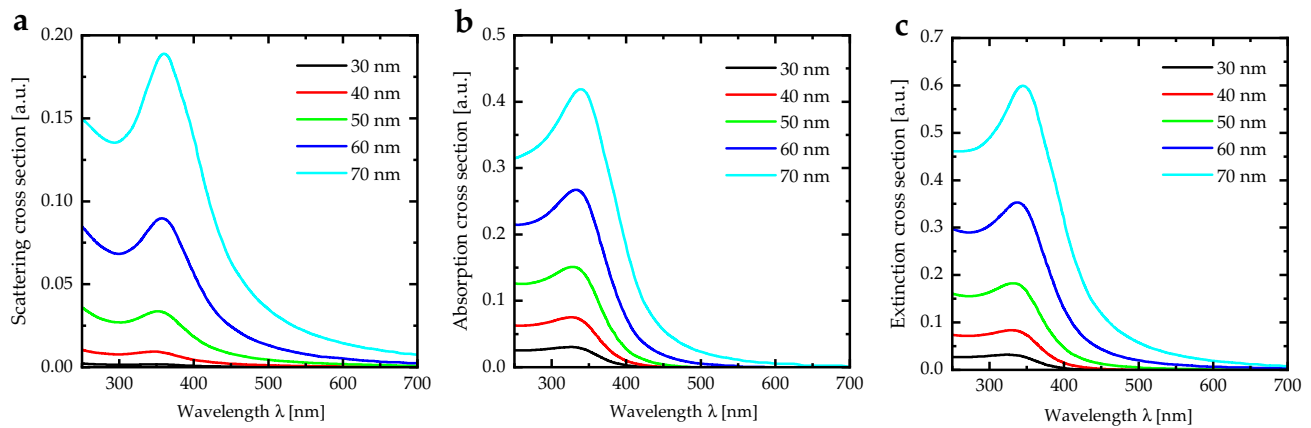


Fig. 5 Analytical optical **a** scattering, **b** absorption, and **c** extinction spectra of AgNPs with different particle sizes (30, 40, 50, 60, and 70 nm)

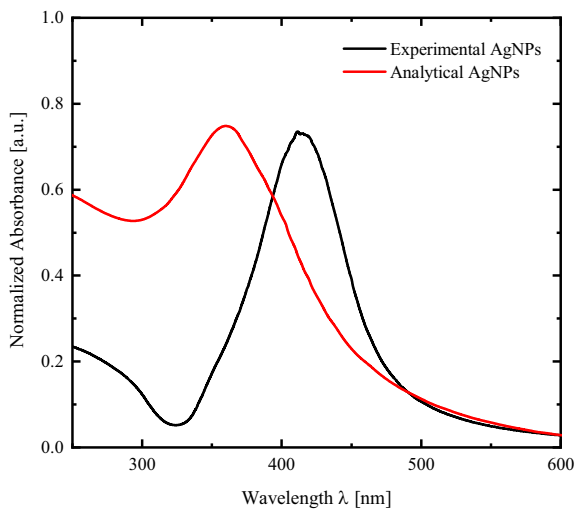


Fig. 6 Analytical optical absorbance spectra compared with the experimental spectra of AgNPs with the same particle size

the AgNPs before interacting with the light wave. Interacting the light wave with the AgNPs reveals exciting free electron densities at the surface, consequently generating collective electron density oscillations at the metal/medium interfaces (Fig. 7c and d). By turning off the light source, the electric field of the electromagnetic wave causes a field perturbation to the free electron cloud revealing empty compensation to the charges near the NP surface, causing coherent vibrational oscillations due to the persistent forces of uncompensated charges on the surface (Fig. 7e and f). After a long time, the AgNPs return to the initial state (Fig. 7g and h) and vibrational resonance damping trend.

Figure 8 shows the excitation of LSPR of the AgNPs at different light wavelengths using the finite-difference time-domain (FDTD) method. The free-electron cloud around the nanoparticle's surface forms coherent vibrational oscillations in the free electron clouds for different wavelengths (200, 300, 400, 500, 600, and 700 nm) of the light source. The highest energy of the coherent oscillations of the free electron clouds occurred at the wavelength of around 300 nm (Fig. 8b), which is consistent with the optical scattering cross-section spectra in Fig. 4.

5 Conclusions

In this work, the optical properties of silver nanoparticles (AgNPs) were explored in Mie theory and compared with the experimental AgNPs using the chemical reduction method. The SEM micrograph shows that the AgNPs have a spherical shape with an average particle size of 30 nm. The XRD patterns confirm that the AgNPs have *fcc* cubic structure with lattice constant $a = 4.155 \text{ \AA}$. In addition, the UV-Vis absorbance spectrum of the AgNPs exhibits a fingerprint peak at 414 nm, which corresponds to the surface plasmon resonance of AgNPs. According to Mie's theory, the wavelength of localized surface plasmon resonance (LSPR) for the spherical AgNPs has a different value compared with the experimental spectrum due to the impurities present in water that results from the preparation process, in addition to the fact that theoretical spectrum takes care

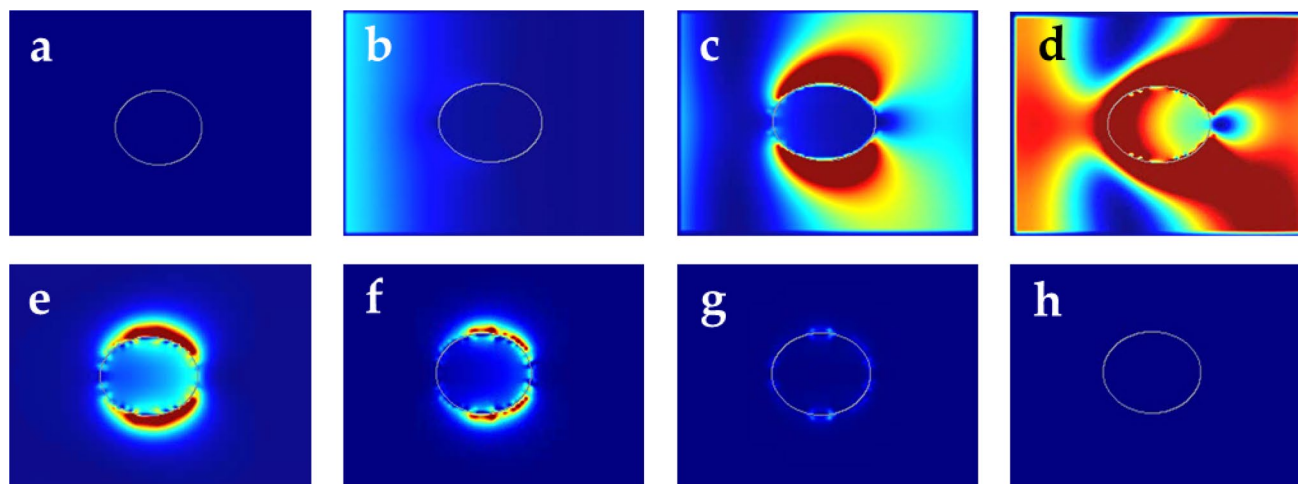


Fig. 7 The excitation of LSPR of the AgNPs using finite-difference time-domain (FDTD) method: **a, b** before interacting the AgNPs with the light wave, **c, d** during the interaction of AgNPs

with the light wave, **e, f** just after the light source is turned off, and **g, h** after a long time from turning off the light

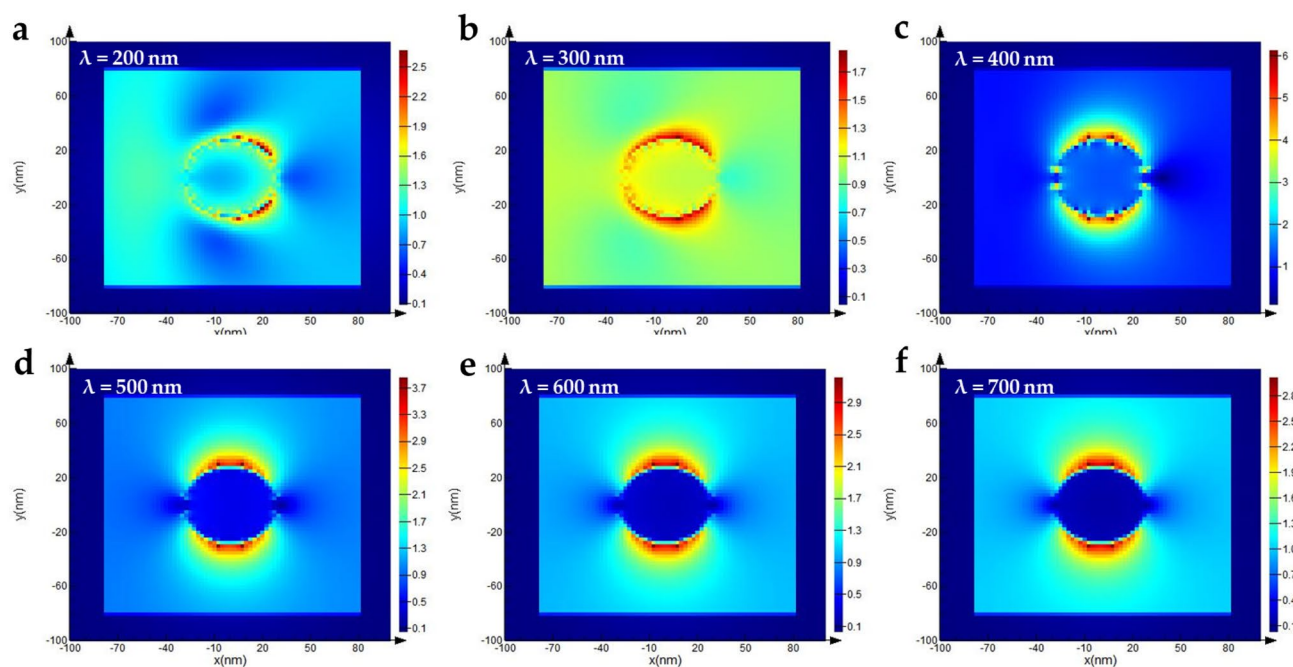


Fig. 8 The excitation of LSPR of the AgNPs using finite-difference time-domain (FDTD) method at wavelength of **a** 200 nm, **b** 300 nm, **c** 400 nm, **d** 500 nm, **e** 600 nm, and **f** 700 nm

of single sized one Ag nanoparticle. In contrast, the experimental spectrum represents many distributed sizes of AgNPs collided in water. Moreover, the excitation of the LSPR of the AgNPs was simulated using

the finite-difference time-domain (FDTD) method at different wavelengths. The results show that spherical AgNPs are the most widely used materials in biosensors, biomedicine, optoelectronic devices, and

solar cells due to their surface plasmon resonances located in the visible spectrum region.

Acknowledgements

The authors would like to acknowledge Jordan University of Science and Technology, the Deanship of Scientific Research, particularly for the support (Research #: 74/2023). We also thank Prof. Mohammad-Ali H. Al-Akhras for helping our members use the biomedical laboratory. The scientific support by the Ministerium für Innovation, Wissenschaft und Forschung des Landes Nordrhein-Westfalen, the Senatsverwaltung für Wirtschaft, Technologie und Forschung des Landes Berlin, and the Bundesministerium für Bildung und Forschung is gratefully acknowledged.

Author contributions

FYA: conceptualization, supervision, writing—review & editing. AAA: data acquisition, writing—original draft. IAA: preparation, data acquisition. ABM: preparation, data acquisition. QMAI-B: conceptualization, computations, and simulation, writing—original draft.

Funding

Open Access funding enabled and organized by Projekt DEAL. This research received no external funding.

Data availability

Not applicable.

Declarations

Conflict of interest The authors declare that they have no known competing financial interests or personal relationships that could have influenced the work reported in this paper.

Consent to participant All authors participate in this work.

Consent for publication All authors agree to publish this work.

Open Access This article is licensed under a Creative Commons Attribution 4.0 International License, which permits use, sharing, adaptation, distribution and reproduction in any medium or format, as long as you give appropriate credit to the original author(s) and the source, provide a link to the Creative Commons licence, and indicate if changes were made. The images or other third party material in this article are included in the article's Creative Commons licence, unless indicated otherwise in a credit line to the material. If material is not included in the article's Creative Commons licence and your intended use is not permitted by statutory regulation or exceeds the permitted use, you will need to obtain permission directly from the copyright holder. To view a copy of this licence, visit <http://creativecommons.org/licenses/by/4.0/>.

References

1. E. Saion, E. Gharibshahi, On the theory of metal nanoparticles based on quantum mechanical calculation. *Malaysian J. Fundam. Appl. Sci.* **7**(1), 6–11 (2011)
2. G. Oberdörster, E. Oberdörster, J. Oberdörster, Nanotoxicology: an emerging discipline evolving from studies of ultrafine particles. *Environ. Health Perspect.* **113**(7), 823–839 (2005)
3. P. Christian, F. Von der Kammer, M. Baalousha, T. Hofmann, Nanoparticles: structure, properties, preparation and behaviour in environmental media. *Ecotoxicology* **17**(5), 326–343 (2008)
4. L. Manna, E.C. Scher, A.P. Alivisatos, Synthesis of soluble and processable rod-, arrow-, teardrop-, and tetrapod-shaped CdSe nanocrystals. *J. Am. Chem. Soc.* **122**(51), 12700–12706 (2000)
5. J.Y. Al-zou'by, F. Alzoubi, A. Migdadi, K. Al-Zboon, Evaluating the impacts of manufactured silver nanoparticles dispersed in various wastewaters on biochemical oxygen demand kinetics of the resulting wastewaters. *Nanotechnol. Environ. Eng.* **8**(1), 119–129 (2023)
6. S. Gurunathan, J.H. Park, J.W. Han, J.-H. Kim, Comparative assessment of the apoptotic potential of silver nanoparticles synthesized by *Bacillus tequilensis* and *Calocybe indica* in MDA-MB-231 human breast cancer cells: targeting p53 for anticancer therapy. *Int. J. Nanomed.* **10**, 4203–4223 (2015)
7. W.-R. Li, X.-B. Xie, Q.-S. Shi, H.-Y. Zeng, O.-Y. You-Sheng, Y.-B. Chen, Antibacterial activity and mechanism

- of silver nanoparticles on *Escherichia coli*. Appl. Microbiol. Biotechnol. **85**(4), 1115–1122 (2010)
8. O.Y. Semchuk, A. Biliuk, O. Havryliuk, A. Biliuk, Kinetic theory of electroconductivity of metal nanoparticles in the condition of surface plasmon resonance. Appl. Surf. Sci. Adv. **3**, 100057 (2021)
 9. J.-Y. Jing, Q. Wang, W.-M. Zhao, B.-T. Wang, Long-range surface plasmon resonance and its sensing applications: a review. Opt. Lasers Eng. **112**, 103–118 (2019)
 10. O. Keller, M. Xiao, S. Bozhevolnyi, Configurational resonances in optical near-field microscopy: a rigorous point-dipole approach. Surf. Sci. **280**(1–2), 217–230 (1993)
 11. J. Jana, M. Ganguly, T. Pal, Enlightening surface plasmon resonance effect of metal nanoparticles for practical spectroscopic application. RSC Adv. **6**(89), 86174–86211 (2016)
 12. D. Paramelle, A. Sadovoy, S. Gorelik, P. Free, J. Hopley, D.G. Fernig, A rapid method to estimate the concentration of citrate capped silver nanoparticles from UV–Visible light spectra. Analyst **139**(19), 4855–4861 (2014)
 13. V. Lozovski, C. Lienau, G. Tarasov, T. Vasyliov, Z.Y. Zhuchenko, Configurational resonances in absorption of metal nanoparticles seeded onto a semiconductor surface. Results Phys. **12**, 1197–1201 (2019)
 14. A. Movsesyan, A.-L. Baudrion, P.-M. Adam, Extinction measurements of metallic nanoparticles arrays as a way to explore the single nanoparticle plasmon resonances. Opt. Express. **26**(5), 6439–6445 (2018)
 15. C.F. Bohren, D.R. Huffman, *Absorption and Scattering of Light by Small Particles* (Wiley, Hoboken, 2008)
 16. Y. Chen, K. Munehika, D.S. Ginger, Dependence of fluorescence intensity on the spectral overlap between fluorophores and plasmon resonant single silver nanoparticles. Nano Lett. **7**(3), 690–696 (2007)
 17. C.M. Copley, S.E. Skrabalak, D.J. Campbell, Y. Xia, Shape-controlled synthesis of silver nanoparticles for plasmonic and sensing applications. Plasmonics **4**, 171–179 (2009)
 18. A. Tao, P. Sinsersuksakul, P. Yang, Polyhedral silver nanocrystals with distinct scattering signatures. Angew Chem. Int. Ed. **45**(28), 4597–4601 (2006)
 19. A. Kheirandish, N.S. Javan, H. Mohammadzadeh, Modified drude model for small gold nanoparticles surface plasmon resonance based on the role of classical confinement. Sci. Rep. **10**(1), 1–10 (2020)
 20. M. Quinten, *Optical Properties of Nanoparticle Systems* (Wiley, Hoboken, 2011)
 21. A. Loiseau et al., Core–shell gold/silver nanoparticles for localized surface plasmon resonance-based naked-eye toxin biosensing. ACS Appl. Mater. Interfaces. **11**(50), 46462–46471 (2019)
 22. S. Liu, G. Chen, P.N. Prasad, M.T. Swihart, Synthesis of monodisperse Au, Ag, and Au–Ag alloy nanoparticles with tunable size and surface plasmon resonance frequency. Chem. Mater. **23**(18), 4098–4101 (2011)
 23. H. Song, H. Zhang, Z. Sun, Z. Ren, X. Yang, Q. Wang, Triangular silver nanoparticle U-bent fiber sensor based on localized surface plasmon resonance. AIP Adv. **9**(8), 085307 (2019)
 24. L. Lu, A. Kobayashi, K. Tawa, Y. Ozaki, Silver nanoplates with special shapes: controlled synthesis and their surface plasmon resonance and surface-enhanced Raman scattering properties. Chem. Mater. **18**(20), 4894–4901 (2006)
 25. A. Amirjani, F. Firouzi, D.F. Haghshenas, Predicting the size of silver nanoparticles from their optical properties. Plasmonics **15**, 1077–1082 (2020)
 26. X. Li, J.J. Lenhart, H.W. Walker, Dissolution-accompanied aggregation kinetics of silver nanoparticles. Langmuir **26**(22), 16690–16698 (2010)
 27. M. Quinten, Local fields close to the surface of nanoparticles and aggregates of nanoparticles. Appl. Phys. B **73**(3), 245–255 (2001)
 28. N. Halas, Playing with plasmons: tuning the optical resonant properties of metallic nanoshells. MRS Bull. **30**(5), 362–367 (2005)
 29. L.B. Sagle, L.K. Ruvuna, J.A. Ruummele, R.P. Van Duyne, Advances in localized surface plasmon resonance spectroscopy biosensing. Nanomedicine **6**(8), 1447–1462 (2011)
 30. B. Tang et al., Application of anisotropic silver nanoparticles: multifunctionalization of wool fabric. J. Colloid Interface Sci. **356**(2), 513–518 (2011)
 31. P. Alivisatos, The use of nanocrystals in biological detection. Nat. Biotechnol. **22**(1), 47–52 (2004)
 32. M.A. Mahmoud, M.A. El-Sayed, Gold nanoframes: very high surface plasmon fields and excellent near-infrared sensors. J. Am. Chem. Soc. **132**(36), 12704–12710 (2010)
 33. H. Ghaforyan, M. Ebrahimzadeh, S.M. Bilankohi, Study of the optical properties of nanoparticles using Mie theory. World Appl. Programm. **5**(4), 79–82 (2015)
 34. J.D. Jackson, *Classical Electrodynamics*, 3rd edn. (Wiley, New York, 1999)
 35. M. Meier, A. Wokaun, Enhanced fields on large metal particles: dynamic depolarization. Opt. Lett. **8**(11), 581–583 (1983)
 36. H. Kuwata, H. Tamaru, K. Esumi, K. Miyano, Resonant light scattering from metal nanoparticles: practical analysis beyond Rayleigh approximation. Appl. Phys. Lett. **83**(22), 4625–4627 (2003)

37. F. Alzoubi et al., Physicochemical characteristics of silver nanoparticles: influence of carbonate alkalinity. *Nanotechnol. Environ. Eng.* **6**(3), 1–9 (2021)
38. W. Cai, V.M. Shalaev, *Optical metamaterials* (Springer, Berlin, 2010), p.6011
39. D.K. Bhui, H. Bar, P. Sarkar, G.P. Sahoo, S.P. De, A. Misra, Synthesis and UV–Vis spectroscopic study of silver nanoparticles in aqueous SDS solution. *J. Mol. Liq.* **145**(1), 33–37 (2009)
40. A. Singh, S. Jha, G. Srivastava, P. Sarkar, P. Gogoi, Silver nanoparticles as fluorescent probes: new approach for bio-imaging. *Int. J. Sci. Technol. Res.* **2**(11), 153–157 (2013)
41. T. Gong, J. Zhang, Y. Zhu, X. Wang, X. Zhang, J. Zhang, Optical properties and surface-enhanced Raman scattering of hybrid structures with Ag nanoparticles and graphene. *Carbon* **102**, 245–254 (2016)

Publisher's Note Springer nature remains neutral with regard to jurisdictional claims in published maps and institutional affiliations.